SUBGRID- OR REYNOLDS STRESS-MODELING FOR THREE-DIMENSIONAL TURBULENCE COMPUTATIONS

By Morris W. Rubesin

NASA Ames Research Center

SUMMARY

A review is given of recent advances in two distinct computational methods for evaluating turbulence fields, namely, statistical Reynolds stress modeling and turbulence simulation, where large eddies are followed in time. It is shown that evaluation of the mean Reynolds stresses, rather than use of a scalar eddy viscosity, permits an explanation of streamline curvature effects found in several experiments. Turbulence simulation, with a new volume averaging technique and third-order accurate finite-difference computing is shown to predict the decay of isotropic turbulence in incompressible flow with rather modest computer storage requirements, even at Reynolds numbers of aerodynamic interest.

INTRODUCTION

It is generally accepted that the Navier-Stokes equations represent the physics of Newtonian fluid flow fields at points in space and time away from sharp discontinuities such as shock waves. The intense shear layers present in turbulence fields, for example, the superlayer, extend over a much larger space than do shock waves, so that it can be expected that the Navier-Stokes equations will apply uniformly over the turbulence fields. Mathematically, turbulence can be considered, then, as the very complex solutions to these equations reflecting their nonlinear character and random sets of initial and boundary conditions. Because of the large set of possible solutions, unique solutions in turbulent flow can be expressed only in terms of averaged quantities over the time and/or space in the expectation that the turbulence is a slowly varying or stationary random process.

The nonlinear character of the equations forces the use of numerical computations, yet attainment of these solutions of the time-dependent Navier-Stokes equations is not possible now or in the foreseeable future. The reason for this is contained in certain features of turbulence that are inimical to finite difference computations. At a point in space, turbulent flow is irregular in time, random in character. In addition, it is three-dimensional and composed of different structures having a large range of length and time scales. To compute the irregularities, it is necessary to employ computational methods that are accurately time dependent. Techniques appropriate to asymptotic solutions that permit overshoots or employ artificial damping cannot be employed because they introduce errors in the instantaneous flow-field development that are likely to grow. The

small-scale dimensions, also, impose numerical stability or accuracy restraints on the allowable advancing time steps in the time-dependent solutions. For example, in an aerodynamic boundary layer, the smallest significant scale requires mesh spacing 10^{-5} of the boundary-layer thickness. The three-dimensionality of the flow, together with the small scale, requires on the order of 10^{17} mesh points to define the flow field of an entire aircraft. The corresponding allowable time step is 1 microsecond of real time. Clearly, these requirements for storage capacity and computer speeds are many orders of magnitude beyond the best of current computers or those contemplated in the foreseeable future. To circumvent these difficulties it is necessary to resort to "turbulence modeling."

The term "turbulence modeling" involves two distinct stages. The first eliminates the small-scale structure of the dependent variable through an averaging of some sort (ensemble, space, or time) that can be carried out with mathematical rigor. The new averaged dependent variables are relatively slow varying so they can be resolved with finite difference methods utilizing mesh dimensions and time intervals compatible with current computers. The nonlinear terms of the basic equations, however, introduce averages of moments of the dependent variables that must be expressed in terms of the averaged quantities retained to avoid a proliferation of dependent variables in excess of the numbers of equations available (the "closure" problem). The manner of doing this is the second stage of the "turbulence modeling" process and in this stage, considerable reliance is placed on comparisons with experimental data to compensate for the "physics" lost in the earlier averaging process.

The name "Statistical Theory of Inhomogenous Turbulence," references 1 and 2, has been applied to the process where averaging is performed at a point in space over a period of time long compared to the time scales of the largest eddies of the turbulence. The method is most suitable to steady-state mean flow fields, although it can be applied as well to flow fields that are slowly varying compared to the large eddy time scales. The resulting dependent variables represent the slowly varying mean flow field and are completely devoid of eddy structure. An alternative method, sometimes called "turbulence simulation," depends on averaging the Navier-Stokes equations over space volumes that are smaller than the largest eddies, but much larger than the tiniest eddies. The new dependent variables (the volume averages) retain their time dependence, but possess scales resolvable by current computer techniques.

The NASA Ames Research Center has been sponsoring research in both of these areas. It is believed that in the short term most practical aerodynamic computations will be based on the statistical theory of turbulence. The aerodynamicist is interested in the mean properties of the flow fields with which he deals so that the behavior of individual eddies is more information than he needs. On the other hand, the modeling hypotheses made in the statistical theory are largely intuitive and supported rather tenuously by a meager supply of data. It hasn't been possible to provide experimental information on all of the multitude of variables that appear in the modeling equations. Turbulence simulation, once verified, will be able to be applied

to a variety of simple flow fields that emphasize particular modeling effects. For example, simulation of homogeneous turbulence decay can shed light on modeled turbulence dissipation in the statistical theory. Simple shear flows can yield information on the diffusion of turbulence kinetic energy, or of pressure fluctuations. Thus, turbulence simulation will provide an excellent basis for guiding statistical modeling. Ultimately, however, the technique of turbulence simulation may go beyond merely providing modeling assistance to statistical theory and become the basis for practical turbulence computation. Inherent in turbulence simulation is its direct evaluation of the large eddies that are characteristic of particular flow fields and modeling of the small scales that are known to be universal in character. These are certainly the elements of a practical prediction scheme.

In this paper, a review will be given of some recent progress in the work sponsored by Ames. The recent contributions to the statistical theory of turbulence were performed at DCW Industries under Contract NAS2-8192. The work in turbulence simulation has been conducted at Stanford University under Grant NGR 05-020-622.

SYMBOLS

e, q^2	specific kinetic energy of turbulence
E	power spectral density
f	function
k	wave number
L	dimension of flow volume
M	turbulence generation grid mesh spacing
p	pressure
S_{ij}	rate of strain of mean motion
t, t^*	time, dummy variable of integration over time period
T	period of integration > > turbulence scale
u, v, w	velocity components in x, y, z directions
u_i	component of velocity in ith direction
u_τ	friction velocity, $\sqrt{\tau_w/\rho}$
U_o	channel mean velocity

x_i	coordinate in ith direction
y	distance normal to surface
Γ	irrotational strain
δ	boundary-layer thickness
δ_{ij}	Kronecker δ
Δ	mesh spacing
Δ_{avg}	dimension for space averaging (see table 1)
ε or ν_T	eddy diffusivity or eddy kinematic viscosity
ν	kinematic viscosity
κ	Von Kármán constant
ρ	density
τ	turbulent shear in boundary layer
$\tau_{ij}, \overline{u_i' u_j'}$	turbulent shear stress in direction i on surface normal to j
τ_w	wall shear
χ	parameter in dissipation term of equation (16)
ω	Saffman's "pseudo vorticity" or dissipation rate

Superscripts:

$(\bar{})$, $< >$	average quantity
$( )'$	instantaneous fluctuating quantity

Subscripts:

e	edge of boundary layer
i,j,k,m,n	tensor indices

STATISTICAL THEORY OF INHOMOGENOUS TURBULENCE

To place the Wilcox contribution (ref. 3) into the proper context of current turbulence modeling it is necessary to review briefly the basis of the statistical theory of turbulence. For simplicity, attention will be confined to incompressible fluid flow. The Navier-Stokes equations are

$$\frac{\partial u_i}{\partial t} + \frac{\partial}{\partial x_j}\left(u_i u_j\right) = -\frac{1}{\rho}\frac{\partial p}{\partial x_i} + \frac{\partial}{\partial x_j}\left(\nu \frac{\partial u_i}{\partial x_j}\right) \tag{1}$$

where the notation of repeated indices represents summation over all the coordinate directions. The local velocity components, or pressure, are written as

$$u_i\left(x_j, t^*\right) = \bar{u}_i\left(x_j, t\right) + u'\left(x_j, t, t^*\right) \tag{2}$$

which allows for slow variation of the mean quantity $\bar{u}_i$ in time t and expresses the fluctuating component within the integration period relative to the mean over the period. The averaging process is defined as

$$\bar{f}\left(x_j, t\right) = \frac{1}{T}\int_{t-T/2}^{t+T/2} f\left(x_j, t^*\right)\, dt^* \tag{3}$$

With equation (2), equation (3) becomes

$$\bar{u}_i\left(x_j, t\right) = \frac{1}{T}\int_{t-T/2}^{t+T/2} \left[\bar{u}_i\left(x_j, t\right) + u'\left(x_j, t, t^*\right)\right] dt^* \tag{4}$$

which reduces to the requirement

$$\frac{1}{T}\int_{t-T/2}^{t+T/2} u'\left(x_j, t, t^*\right)\, dt^* = 0 \tag{5}$$

When equation (1) is averaged according to equations (3) and (5), there results

$$\frac{\partial \bar{u}_i}{\partial t} + \frac{\partial \bar{u}_i \bar{u}_j}{\partial x_j} = -\frac{1}{\rho}\frac{\partial \bar{p}}{\partial x_i} + \frac{\partial}{\partial x_j}\left(\nu \frac{\partial \bar{u}_i}{\partial x_j} - \overline{u_i' u_j'}\right) \tag{6}$$

Before equation (6) can be solved it is necessary to express the moments $\overline{u_i' u_j'}$ (the Reynolds stresses) in terms of the mean flow $\bar{u}_j$ and the characteristics of the turbulence. If equation (1) is manipulated to yield a differential equation for $\overline{u_i' u_j'}$, reference 1, in addition to terms containing $\overline{u_i' u_j'}$ and $\bar{u}_j$, new quantities involving quadratures of u_j' and p' and $\overline{u_i' u_j' u_k'}$ appear. An additional set of equations for $\overline{u_i' u_j' u_k'}$ leads to many new higher moments. In general, equations for higher moments lead to more new dependent variables than new equations. The means of stopping this diverging process is achieved through "closure" hypothesis.

The most widely used closure method has been based on the concept of an eddy viscosity; for example, where it is hypothesized that the turbulence Reynolds stresses $\overline{u_i'u_j'}$ are proportional to the rate of strain of the mean flow, with the factor or proportionality, the eddy viscosity, being a scalar quantity. The similarity to Stokes stress relations in laminar flow and the role of viscosity is evident. With the eddy viscosity, ε,

$$\overline{u_i'u_j'} = 2\varepsilon S_{ij} - 2/3\,\delta_{ij}e \tag{7}$$

where the mean rates of strain, S_{ij}, are

$$S_{ij} = \frac{1}{2}\left(\frac{\partial \bar{u}_i}{\partial x_j} + \frac{\partial \bar{u}_j}{\partial x_i}\right) \tag{8}$$

for an incompressible fluid. Turbulence kinetic energy, e, is

$$e = \frac{1}{2}\overline{u_i'u_i'} \tag{9}$$

The earliest theories, due to Prandtl, expressed

$$\varepsilon = \varepsilon\left(x_2, S_{ij}, \kappa\right) \tag{10}$$

through an algebraic expression with κ an empirical constant. Since this "closed" the problem at the level of equation (6), it has been termed "first-order closure." The method was quite successful for pipe flows and boundary layers where changes occurred gradually. In fact, extensions of this method to compressibility has provided several decades of usefulness through accurate prediction of skin friction at high Mach numbers for two-dimensional aerodynamic configurations, evaluations of aerodynamic heating phenomena, and the assessment of concepts such as transpiration cooling or ablation for alleviating the effects of aerodynamic heating. The method is most accurate when restricted to simple shapes. Its cost effectiveness in numerical computations, however, has made its use attractive in heuristic investigations even for conditions where it cannot be expected to be accurate, namely, the zones of interaction between a shock wave and a turbulent boundary layer that is the topic of several of the papers in this conference.

For more general body shapes, especially those having rapidly varying boundary-layer edge conditions, the introduction of rate processes in the development in the turbulence is necessary. Here the eddy viscosity is expressed as a function of two turbulence quantities equivalent to velocity and time or length scales. As an example, the Saffman model (ref. 4) sets

$$\varepsilon = \frac{e}{\omega} = \frac{\text{turbulent specific kinetic energy}}{\text{"pseudo vorticity" or "dissipation rate"}} \tag{11}$$

where

$$\frac{De}{Dt} = f_1\left(e,\omega,S_{ij}\right) \tag{12}$$

and

$$\frac{D\omega^2}{Dt} = f_2\left(e,\omega,S_{ij}\right) \tag{13}$$

The functions f_1 and f_2 are not the exact terms that can be derived from equation (1), but are "modeled" to express the physical quantities actually present, rates of turbulence production, dissipation, and diffusion, in functional forms containing a closed set of dependent variables. These functional forms are dimensionally consistent and contain empirical constants that are expected to be insensitive to the character of individual flow fields. A review of a large number of such two-equation models, where the modeling takes place in the equations for the turbulence quantities and is called "second-order closure," is given in reference 5.

There are flow conditions, especially cases of three-dimensional flows, where the concept of the scalar eddy viscosity fails. For these conditions it is necessary to evaluate the Reynolds stresses $\overline{u_i'u_j'}$ directly. Several investigators have devised models of the direct Reynolds stress equations, references 6 through 8. The method described in this paper possesses desirable features. It is relatively simple, reducing to the simple Saffman eddy viscosity model when flow conditions permit, and it is easily extendable to compressible flows through the use of mass averaged dependent variables, reference 9. Furthermore, as is shown later, it has proved to be quite successful in explaining the streamline curvature effects documented in Bradshaw's monograph, reference 10.

The equation representing the Reynolds stresses of equation (6) can be written exactly as

(Convection) (Production) (Dissipation)

$$\frac{\partial \tau_{ij}}{\partial t} + \bar{u}_k \frac{\partial \tau_{ij}}{\partial x_k} = - \tau_{ik} \frac{\partial \bar{u}_j}{\partial x_k} - \tau_{jk} \frac{\partial \bar{u}_i}{\partial x_k} + 2\nu \overline{\frac{\partial u_i'}{\partial x_k} \frac{\partial u_j'}{\partial x_k}}$$

(Tendency to Isotropy)

$$- \overline{\frac{p'}{\rho} \left[\frac{\partial u_j'}{\partial x_i} + \frac{\partial u_i'}{\partial x_j} \right]}$$

(Turbulent Diffusion of Pressure)

$$+ \frac{\partial}{\partial x_k} \left[\delta_{ik} \overline{u_j' \frac{p'}{\rho}} + \delta_{jk} \overline{u_i' \frac{p'}{\rho}} \right]$$

(Molecular and Turbulent Diffusion of Stress)

$$+ \frac{\partial}{\partial x_k} \left[\nu \frac{\partial \tau_{ij}}{\partial x_k} + \overline{u_k' u_i' u_j'} \right] \qquad (14)$$

where

$$\tau_{ij} = - \overline{u_i' u_j'} \qquad (15)$$

The terms on the left represent the convection of the Reynolds stresses. The first two terms on the right are the production terms; for example, where the mean flow strain interacts with the Reynolds stresses. The third term on the right is the dissipation term. It depends on quadratures of the instantaneous velocity gradients and therefore is largely dependent on the small scales of the turbulence. The next term, involving correlations of pressure and velocity gradient correlations, permits exchange between the individual Reynolds stresses and is termed the "tendency toward isotropy." This term vanishes for incompressible flow when equation (14) is contracted to yield an equation for the turbulent kinetic energy. The next term is the diffusion of pressure fluctuations by turbulence. Finally, the last term on the right, a divergence form, represents the diffusion of the Reynolds stresses by molecular and turbulent mechanisms. Dave Wilcox of DCW Industries models the Reynolds stress equation as

(Convection) (Production) (Dissipation)

$$\frac{\partial \tau_{ij}}{\partial t} + \bar{u}_k \frac{\partial \tau_{ij}}{\partial x_k} = - \tau_{ik} \frac{\partial \bar{u}_j}{\partial x_k} - \tau_{jk} \frac{\partial \bar{u}_i}{\partial x_k} + \frac{2}{3} \beta^* \left[1 - \chi + \chi^2 \right] e\omega\delta_{ij}$$

(Tendency to isotropy) (Production redistribution)

$$- \lambda^* \omega \left[\tau_{ij} + \frac{2}{3} e\delta_{ij} \right] + 4 \frac{e}{\omega} \left[S_{im} S_{mj} - \frac{1}{3} S_{mn} S_{mn} \delta_{ij} \right]$$

(Molecular and turbulent diffusion)

$$+ \frac{\partial}{\partial x_k} \left[\left(\nu + \sigma^* \frac{e}{\omega} \right) \frac{\partial \tau_{ij}}{\partial x_k} \right] \qquad (16)$$

where

$$\chi = \sqrt{\frac{2 S_{mn} S_{mn}}{\beta^* \omega^2}}$$

The turbulent dissipation rate, ω, is given by

$$\frac{\partial \omega^2}{\partial t} + \bar{u}_k \frac{\partial \omega^2}{\partial x_k} = \left[\alpha \sqrt{\frac{\partial \bar{u}_i}{\partial x_j} \frac{\partial \bar{u}_i}{\partial x_j}} - \beta\omega \right] \omega^2 + \frac{\partial}{\partial x_k} \left[\left(\nu + \sigma \frac{e}{\omega} \right) \frac{\partial \omega^2}{\partial x_k} \right] \qquad (17)$$

after Saffman, reference 4. The turbulent kinetic energy, e, obtained as the contraction of equation (16), is

$$\frac{\partial e}{\partial t} + \bar{u}_k \frac{\partial e}{\partial x_k} = \left[\alpha^* \sqrt{2 S_{mn} S_{mn}} - \beta^* \omega \right] e + \left[\tau_{ij} - 2 \frac{e}{\omega} S_{ij} \right] \frac{\partial \bar{u}_i}{\partial x_j}$$

$$+ \frac{\partial}{\partial x_k} \left[\left(\nu + \sigma^* \frac{e}{\omega} \right) \frac{\partial e}{\partial x_k} \right] \qquad (18)$$

where

$\alpha = 0.2638 \qquad \beta^* = \alpha^{*2} = 8/81 = .0988$

$\beta = 0.18$

$\sigma = 0.50 \qquad \sigma^* = 0.5 \qquad \lambda^* = (9/2)\ \beta^*$

These constants are consistent with the Saffman formulation. Wilcox introduced an additional constant λ^*, which he evaluated by requiring the normal stresses in a flat plate boundary layer to have the ratio $\overline{u'^2} : \overline{v'^2} : \overline{w'^2}$ equal to 4:2:3 to conform to experiment.

A comparison of the exact equation (14) and the modeled equation (16) indicates that modeling has been applied to all the terms other than turbulence production. The form of the modeled terms are expressed in a limited invariant tensor form, as compared to reference 7. Consistent with the Saffman model, the dissipation term does not represent the energy dissipated by molecular processes at the smallest scales, but rather accounts for the energy cascaded to the smallest eddies by the larger eddies. Saffman assumed that the scales of the smallest eddies adjust to accommodate the turbulence passed to them, and thereby avoids the need for two length scales. The quantity $1 - \chi + \chi^2$ in equation (16) is always greater than zero, giving dissipation its proper sign. One can consider that the terms labeled "tendency to isotropy" and "production redistribution" together model the "tendency to isotropy" term of equation (14) as the contraction of all these terms is zero. The current Wilcox model neglects the "turbulent diffusion of pressure." Finally, the "turbulent diffusion of stress," the third order correlation, is modeled through an eddy viscosity assumption supplemented by an effective turbulent Prandtl number, σ^*.

One of the first problems to which this model was applied was the effect of streamline curvature in attached turbulent boundary layers. Considered was a constant pressure flow over a curved surface having a radius of curvature R in the plane of the two-dimensional mean flow. From a perturbation solution of equations (6) and (16) to (18) corresponding to the wall region of the boundary layer, Wilcox found that mean velocity could be expressed in the usual wall layer dimensionless quantities as

$$\left(1 - \phi \frac{y}{R}\right) \frac{u}{u_\tau} = \frac{1}{\kappa} \log \frac{u_\tau y}{\nu} + \text{Constant} \tag{19}$$

with

$$\phi = 15.4 \tag{20}$$

The corresponding turbulence quantities were found to be

$$e = \frac{u_\tau^2}{\alpha^*} \left[1 + 0 \left(\frac{y}{R} \log \frac{u_\tau y}{\nu} \right)^2 \right] \tag{21}$$

$$\omega = \frac{u_\tau}{\alpha^* \kappa y} \left[1 + 2.4 \frac{y}{R} \log \frac{u_\tau y}{\nu} + \ldots \right] \tag{22}$$

$$\overline{u'^2} = \frac{8}{9}\frac{u_\tau^2}{\alpha^*}\left[1 + 3\frac{y}{R}\log\frac{u_\tau y}{\nu} + \ldots\right] \tag{23}$$

$$\overline{v'^2} = \frac{4}{9}\frac{u_\tau^2}{\alpha^*}\left[1 - 10\frac{y}{R}\log\frac{u_\tau y}{\nu} + \ldots\right] \tag{24}$$

$$\overline{w'^2} = \frac{6}{9}\frac{u_\tau^2}{\alpha^*}\left[1 + \frac{8}{3}\frac{y}{R}\log\frac{u_\tau y}{\nu} + \ldots\right] \tag{25}$$

In addition, the local shear turned out to be expressible in terms of an eddy viscosity

$$\tau = \frac{1}{\lambda^*}\frac{\overline{v'^2}}{\omega}\frac{\partial \bar{u}}{\partial y} \tag{26}$$

These results are very significant in several ways. First, the law of the wall expression, equation (19), has the same form found to correlate experimental data measured over a curved wall. The value of ϕ found experimentally by R. N. Meroney, was $\phi \cong 12$, which is in reasonable agreement with the modeled value of equation (20). Furthermore, the specific kinetic energy of the turbulence, equation (21), is shown to be relatively unaffected by the streamline curvature. Again, this is in agreement with experimental data for corresponding flow conditions where So and Mellor, reference 11, found ϵ_{max}/u_τ^2 unaffected by curvature for convex walls. A comparison of equations (23) through (25) shows that streamline curvature affects the individual normal stresses differently. The normal stresses along and across the surface increase, while the normal stress perpendicular to the surface decreases and in an amount larger than the others. The difference in sign of the behavior of the normal stresses demonstrates why the specific kinetic energy remains essentially constant. It is interesting that the expression equation (26) for the shear stress, τ, shows an eddy viscosity form, but where the characteristic turbulence velocity scale is not the specific kinetic energy, e, reference 4, but the normal stress $\overline{v'^2}$. The sensitivity of $\overline{v'^2}$ to the effects of streamline curvature and its direct effect on the shear explains much of the streamline curvature effect discussed by Bradshaw, reference 10.

Another comparison of the Wilcox Reynolds stress computations with experimental data is shown in figure 1. These data were obtained by Bradshaw, reference 12, in a turbulent boundary layer on a flat plate on which an adverse pressure was suddenly applied. The data include profiles of the three individual normal Reynolds stresses, the shear stress, the specific kinetic energy, and the mean velocity at a station 1.52 m after the adverse pressure gradient was applied. To initiate the computations, extensive use was made of the Bradshaw mean flow and hot-wire data at the start of the adverse pressure gradient. The initial mean velocity and

specific kinetic energy profiles were directly obtained from the data. The ω profile was deduced from the measured turbulent shear stress and mean velocity profiles by utilizing the eddy viscosity relationship

$$\tau = \rho \frac{e}{\omega} \frac{\partial \bar{u}}{\partial y} \tag{27}$$

Because the shear τ and $\partial\bar{u}/\partial y$ both approach zero near the boundary-layer edge, the determination of ω there becomes uncertain and is a source of error. The value of ω found at the boundary layer edge and used at all stations as a boundary condition on equation (17) was $\omega_e = 10^{-4}\, u_e^2/\nu$.

The Reynolds stress theory, shown in figure 1 as the solid lines, does a good job in predicting the maximum levels of the normal stresses, however, the shapes of the profiles for $\overline{u'^2}$ and $\overline{w'^2}$ are missed badly. In contrast, the $\overline{v'^2}$, the normal stress perpendicular to the surface, is predicted quite well everywhere in the boundary layer. It should be noted that after experiencing the adverse pressure gradient, the ratio $\overline{u'^2}_{max} : \overline{v'^2}_{max} : \overline{w'^2}_{max}$ is 9:5:7, which the theory seems to predict without modification of the constant λ^*. The comparisons with the data for the shear stress, turbulent energy, and mean velocity also contain the predictions by the eddy viscosity model of Saffman indicated by the dashed lines. Because the Wilcox model relies so heavily on the Saffman model, it is not surprising that the two theories give such similar results, especially at a station where the turbulence is nearly in equilibrium. For these quantities, the predictions, while encouraging, yield results that can stand improvement.

From this brief comparison with data, it can be concluded that the Wilcox Reynolds stress model with second-order closure predicts the effects of streamline curvature rather accurately in the wall region of a boundary layer. Of the normal stresses, the $\overline{v'^2}$ is most strongly affected. This, in turn, affects the shear stress since in this region $\tau \simeq 1/\lambda^*(\overline{v'^2}/\omega)(\partial\bar{u}/\partial y)$. The latter is a most important practical result in that it shows that current eddy viscosity models with $\overline{v'^2}$ replacing the turbulence energy as the characteristic turbulence velocity still may apply in regions of streamline curvature. Despite the success of the model near the surface, modeling improvements are required to increase the accuracy of predictions away from the surface. Perhaps the diffusion of pressure fluctuations by turbulence cannot be neglected. Further, it may be necessary to modify the constants of the Saffman theory for particular flow fields to enhance accuracy at the sacrifice of generality.

TURBULENCE SIMULATION

The turbulence simulation calculations to be described here are being conducted at Stanford University, with Profs. William Reynolds and Joel Ferziger as the principal investigators. The primary goal of the Stanford activity is to derive turbulence simulation techniques ultimately suitable for use with compressible fluids and complex aerodynamic configurations. The initial stages of the program, however, have been confined to very simple

flow fields and to incompressible fluids so that comparisons of the techniques employed could be made with the results of other workers in turbulence simulation and with certain fundamental experiments based on hot-wire measurements.

The program began with a careful reconsideration of the volume averaging process by Leonard, reference 13. The new averaged equations contained second order terms that required finite difference methods with truncation errors fourth order in space and second order in time. These equations have been used to study the decay of incompressible, isotropic flow with different numerical techniques and alternative models for subgrid closure. The work is being extended, currently, to flows with irrotational plane strain, simple shear, and a jet into an axial stream.

Table 1 and figure 2 compare the bases of the averaging technique devised by Leonard with those of the more conventional approach. The averaged Navier-Stokes equation shown at the top of table 1 is common to both methods. The dependent variables, however, have different meaning. The conventional average quantity is a uniformly weighted average over a volume of dimension Δ_j around the point x_j. The volume dimension Δ_j is customarily set equal to the finite difference mesh dimension. The Leonard average is weighted toward the center of the averaging volume x_j as $G(x_j-x_j')$ is required to decay to a zero value with increasing distance x_j-x_j'. Specifically, in most of the numerical work a Gaussian weighting function has been adopted with Δ_{avg}, not necessarily set equal to the mesh spacing, as a parameter. In either averaging method, the gradient of an average equals the average of a gradient. Key to the difference in the averaging techniques is the manner in which the local velocity vector is divided into the resolvable and irresolvable eddy contributions. This is shown mathematically in table 1 and diagramatically in the figure 2. In the conventional case, the resolvable velocity is identified with the mean velocity in the box so that the irresolvable component, then, averages to zero. With this definition the averaged nonlinear moment can be expressed as the product of the individual average velocity components plus the Reynolds stress. It is emphasized that this Reynolds stress is time dependent, just as are the averaged velocities related to the large eddies. In Leonard averaging, the resolvable component of velocity $\bar{u}_i$ is treated as a continuously varying quantity across the averaging volume, and the irresolvable fluctuations are defined relative to the local $\bar{u}_i$. The averaged nonlinear moment is much more complex containing a term representing the divergence of the quadrature of the mean velocities as well as a series of quantities that are identified in the aggregate as a Reynolds stress. The modeling of the Reynolds stresses, although they are inherently different quantities, is the same functionally in either method. The Reynolds stress of the unresolved components, R_{ij}, for either averaging method is expressed in terms of an eddy viscosity and the instantaneous strain of the resolved eddies. The definition of the eddy viscosity follows Smagorinsky, reference 14, where the length scale is set equal to the mesh spacing and the frequency scale is related to the root of the sum of the squares of all the strain elements. An alternative eddy viscosity has been utilized by the Stanford group wherein the frequency scale depends on the vorticity of the resolved eddies,

having the advantage of going to zero where the flow is irrotational. The latter approach may aid in defining the boundaries between turbulent and nonturbulent, irrotational flow regions.

The main contribution resulting from the Leonard averaging process is the addition of the term $\Delta^2_{avg}/24(\partial^2/\partial x_j^2)(\bar{u}_i\bar{u}_j)$ to the expression for the averaged moment. Since this term is contained within an operator $\partial/\partial x_j$ it is of third order when expressed in finite difference form. To retain the significance of this term, the Stanford group was forced to adopt finite difference methods with fourth-order truncation errors in space, reference 15. The usual second-order finite differencing in time was retained.

The results of some of the Stanford computations of the decay of homogeneous, isotropic turbulence are shown in figures 3 through 6. The data used for comparison were measured by Compte-Bellot and Corrsin, reference 16, in a uniform flow behind a turbulence generating grid at a Reynolds number per foot of about 200,000. The experimental three-dimensional turbulent energy spectrum at a fixed position in the channel downstream of the grid, shown in figure 3, was adopted as the initial conditions for the calculations. Because the mean flow rate is uniform, the distance along the channel serves as the independent variable of the problem and can be expressed in time as tU_o/M, where M is the mesh spacing of the turbulence generation grid. At the higher wave numbers, the spectrum possesses the $k^{-5/3}$ distribution expected of homogeneous, isotropic turbulence according to the theory of Kolmogoroff, reference 17. The vertical lines in figure 3 define the range of wave numers, k, resolved in the calculations by mesh spacings where each side of the calculational volume is divided into 16 or 32 parts. The lower bound results from the imposition of periodic boundary conditions on opposite faces of the cubic volume, so that

$$k_{min} = \frac{2\pi}{L} \tag{28}$$

where L is the length of the side of the cube. For the cube divided in 16^3 parts, L is taken to be 24 cm. For the cube divided in 32^3 parts, L is 32 cm. The corresponding k_{min}, from equation (28), are 0.26 cm^{-1} and 0.2 cm^{-1}, respectively. The upper value of the resolved k is dependent on the computational mesh dimension, being smaller for the 32^3 mesh division. Within these bounds, the 32^3 mesh division can resolve eddies that account for 80% of the total turbulence energy, whereas the 16^3 mesh division only accounts for about 71% of the energy.

The next three figures (4 to 6) show the evolution of the turbulence spectra at times, or distances beyond the turbulence generating grid, after the initial value set at the farthest upstream test station. All of the figures represent the case of the cube divided into 16^3 parts and with computational mesh spacings of 1.5 cm. The results found from the 32^3 case showed no marked improvements in the calculations. The computation was initiated by expressing the turbulence in a 3-dimensional Fourier series. The Fourier transform of this velocity series to wave-number space then was matched directly to the experimental energy spectrum to give the magnitude of the

coefficients corresponding to each wave-number vector. These vectors were then randomly oriented with a random number generator. Finally, an inverse Fourier transform was applied to achieve the initial turbulence field compatible with the measured energy in physical space. The decay of the turbulence field was then computed using the time-dependent methods described earlier.

Figure 4 shows the effect of setting $\Delta_{avg} = 0$ and utilizing the Smagorinsky subgrid eddy viscosity model (see table 1) in the computations. The dashed lines represent the data at the initial time, $tU_o/M = 42$, and a subsequent time, $tU_o/M = 98$. The computed spectra are represented with the solid lines. Initially the computations are made to agree with the $tU_o/M = 42$ data line as described earlier. The development of the spectra after this time is the test of the method and the subgrid model. From table 1, it is noted that with $\Delta_{avg} = 0$, the weighting function in the Leonard averaging is a Dirac function and the averaged Navier-Stokes equation is formally the same as in conventional averaging, although the meaning of the dependent variable $\bar{u}_i$ is different. For $\Delta_{avg} = 0$, as time progresses, a piling up of energy occurs at the high wave-number end that becomes progressively worse.

Figure 5 shows the evolution of the energy spectrum if the averaging volume dimension is increased to equal to the computational mesh dimensions, $\Delta_{avg} = \Delta$. Again, the Smagorinsky eddy viscosity model is used for the subgrid Reynolds stresses. Note that the dashed lines representing the data are different from those in the previous figure because the data have been averaged according to the Leonard formula with $\Delta_{avg} = \Delta$ in order to express the data in the same dependent variables as in the computations. The unusually high energy at the high wave numbers evident in the previous figure for $\Delta_{avg} = 0$ at $tU_o/M = 98$ is reduced here for $\Delta_{avg} = \Delta$. Finally, in figure 6, the results of using $\Delta_{avg} = 2\Delta$ are shown. Again the data have been averaged to make the data and computation dependent variables correspond. The dashed line at $tU_o/M = 98$ is the averaged data. The points in symbols show the computed spectrum at $tU_o/M = 98$ for both the Smagorinsky and vorticity models of the subscale eddy viscosity (see table 1). There is little to choose between the different models for this example. Both show excellent agreement with the data, and the piling-up of the calculations at high wave number is no longer evident. It appears that the use of $\Delta_{avg} = 2\Delta$ is most appropriate for this type of problem and that the additional term in the Leonard averaging process acts to redistribute the energy within the spectrum in an appropriate manner.

The last figure, figure 7, shows some early results of computations of the distortion of homogeneous turbulence by irrotational plane strain. A field of homogeneous isotropic, turbulence is passed through the transition section shown schematically in the upper left of the figure. The cross-sectional area is constant so that $\bar{w}$, the mean velocity in the z direction remains constant. In the center portion, the walls perpendicular to the y-axis move in to just balance the outward movement of the walls perpendicular to the x-axis, resulting in a constant irrotational plane strain of the mean flow. Downstream of the transition region, the walls again become parallel.

The development of the mean normal stresses with distance along the channel as computed by turbulence simulation is shown in the lower portion of the figure. Again, a cubic volume of 16^3 mesh points was employed. At station 0 the turbulence, initiated as described earlier for the decay problem, is nearly isentropic $\overline{u'^2} = \overline{v'^2} \cong \overline{w'^2}$. In the region of constant irrotational strain, the normal stress in the expanding direction, $\overline{u'^2}$, diminishes, whereas, $\overline{v'^2}$, in the contracting direction increases. The axial normal stress remains relatively unchanged. In the downstream parallel section, the turbulence appears to be returning to isotropy as expected, but very slowly.

The results of turbulence simulation calculations described here are most encouraging. Through adjustment of the volume-averaging process and the use of higher order finite differencing, it has been possible to accurately predict the decay rate and spectral content of the large eddies of homogeneous, isotropic turbulence in incompressible flow. No difficulties have been encountered for the decaying type of flow with the standard subgrid modeling techniques. In addition, early attempts at handling more complex flows are yielding reasonable results with relatively little extra effort. Perhaps the most important result to date is the attainment of accurate turbulence prediction at Reynolds numbers of aerodynamic interest with the rather small number of mesh points employed.

CONCLUDING REMARKS

The success of the Reynolds stress modeling in the statistical theory of turbulence within a boundary layer in the immediate vicinity of the wall is most encouraging. Although improvements in modeling are still required for the wake region of the boundary layer, a way of doing this other than by reasoned intuition seems to be close at hand through turbulence simulation. In the near future, significant advances can be expected through the intersection of these seemingly disparate approaches to the evaluation of turbulence flows. Solutions to simple problems at aerodynamic Reynolds numbers appear to be possible currently as computer storage requirements and subgrid modeling do not seem to be as critical as was anticipated earlier.

REFERENCES

1. Rotta, J.: Statistische Theorie nichthomogener Turbulenz. 1. Mitteilung. Z. Phys., Bd. 129, 1951, pp. 547-572. (Available as NASA TT F-14560).

2. Rotta, J.: Statistische Theorie nichthomogener Turbulenz. 2. Mitteilung. Z. Phys., Bd. 131, 1951, pp. 51-77. (Available as NASA TT FF-11696).

3. Wilcox, D. C. and Chambers, T. L.: Streamline Curvature Effects on Turbulent Boundary Layers. DCW Industries Report DCW-R-04-01, Feb. 1975.

4. Saffman, P. G.: A Model for Inhomogeneous Turbulent Flow. Proc. Roy. Soc. Lond. A, vol. 317, 1970, pp. 417-433.

5. Launder, B. E., and Spalding, D. B.: Mathematical Models of Turbulence. Academic Press, London, 1972.

6. Daly, B. J., and Harlow, F. H.: Transport Equations in Turbulence, Physics of Fluids, vol. 13, no. 11, Nov. 1970, pp. 2634-2649.

7. Donaldson, C duP., Sullivan, R. D., and Rosenbaum, H.: A Theoretical Study of the Generation of Atmospheric Clear Air Turbulence, AIAA Journal, vol. 10, no. 2, Feb. 1972, pp. 162-170.

8. Hanjalac, K. and Launder, B. E.: A Reynolds Stress Model of Turbulence and its Application to Thin Shear Flows. J. Fluid Mech., vol. 52, pt. 4, 1972, pp. 609-638.

9. Rubesin, M. W. and Rose, W. C.: The Turbulent Mean-Flow, Reynolds Stress, and Heat-Flux Equations in Mass-Averaged Dependent Variables. NASA TM X-62,248, March 1973.

10. Bradshaw, P.: Effects of Streamline Curvature on Turbulent Flow. AGARD-AG-169 (1973).

11. So, R. M. C. and Mellor, G. L.: An Experimental Investigation of Turbulent Boundary Layers Along Curved Surfaces. NASA CR-1940, 1972.

12. Bradshaw, P.: The Response of a Constant-Pressure Turbulent Boundary Layer to the Sudden Application of an Adverse Pressure Gradient. NPL Aero Rep. 1219, Brit. A.R.C., Jan. 6, 1967.

13. Leonard, A.: Energy Cascade in Large-Eddy Simulations of Turbulent Fluid Flows. Advances in Geophysics, vol. 18A, F. N. Frankiel and R. E. Munn (Ed.) Academic Press, N.Y., 1974.

14. Smagorinsky, J.: General Circulation Experiments with the Primitive Equation: I The Basic Experiment. Monthly Weather Review, vol. 91, No. 3, Mar. 1963, pp. 99-164.

15. Shanaan, S. and Ferziger, J. H.: A Direct Method of Solution of Poisson Equation Accurate to Fourth Order. Report No. TF-3, Stanford University, August 1974.

16. Compte-Bellot, G. and Corrsin, S.: Simple Eulerian Time Correlation of Full- and Narrow-Band Velocity Signals in Grid-Generated, "Isotropic" Turbulence. J. Fluid Mech., vol. 48, pt. 2, July 28, 1971, pp. 273-337.

17. Hinze, J. O.: Turbulence, McGraw-Hill Book Co., New York, 1959.

TABLE 1. COMPARISON OF CONVENTIONAL AND LEONARD AVERAGING

$$\frac{\partial \bar{u}_i}{\partial t} + \frac{\partial}{\partial x_j}(\overline{u_j u_i}) = -\frac{1}{\rho}\frac{\partial \bar{p}}{\partial x_i} + \frac{\partial}{\partial x_j}\left(\nu \frac{\partial \bar{u}_i}{\partial x_j}\right)$$

CONVENTIONAL	LEONARD
$\bar{f}(x_j) = \frac{1}{\Delta_j}\int_{x_j-\Delta_j/2}^{x_j+\Delta_j/2} f(x_j')dx_j'$	$\bar{f}(x_j) = \int_{-\infty}^{+\infty} G(x_j-x_j')\, f(x_j')dx_j'$

$$\frac{\partial \bar{f}}{\partial x_j} = \frac{\partial \bar{f}}{\partial x_j}$$

$$G(x_j-x_j') = \left\{\sqrt{\frac{6}{\pi}}\frac{1}{\Delta_{avg}}\right\}^2 \exp\left\{-\frac{6(x_j-x_j')^2}{\Delta_{avg}^2}\right\}$$

$u_i(x_j) = \bar{u}_i(x_j) + u_i'(x_j,x_j')$	$u_i(x_j') = \bar{u}_i(x_j') + u_i'(x_j')$
$\overline{u_i'} = 0$	$\overline{u_j'} \neq 0$
$\overline{u_i u_j} = \bar{u}_i\bar{u}_j + \underbrace{\overline{u_i'u_j'}}_{R_{ij}}$	$\overline{u_i u_j} = \bar{u}_i\bar{u}_j + \frac{\Delta_{avg}^2}{24}\frac{\partial^2}{\partial x_j^2}(\bar{u}_i\bar{u}_j) + \underbrace{\overline{u_i'\bar{u}_j} + \overline{\bar{u}_i u_j'} + \overline{u_i'u_j'}}_{R_{ij}}$

WHERE $R_{ij} = -2\nu_T S_{ij} + \frac{1}{3}R_{ii}$ $\qquad S_{ij} = \frac{1}{2}\left(\frac{\partial \bar{u}_i}{\partial x_j} + \frac{\partial \bar{u}_j}{\partial x_i}\right)$

SMAGORINSKY $\qquad \nu_T = C_S\Delta^2(2S_{mn}S_{mn})^{1/2}$

VORTICITY $\qquad \nu_T = C_V\Delta^2(\bar{\omega}_n\bar{\omega}_n)^{1/2}$ $\qquad \bar{\omega}_k = \left(\frac{\partial \bar{U}_i}{\partial x_j} - \frac{\partial \bar{U}_j}{\partial x_i}\right)$

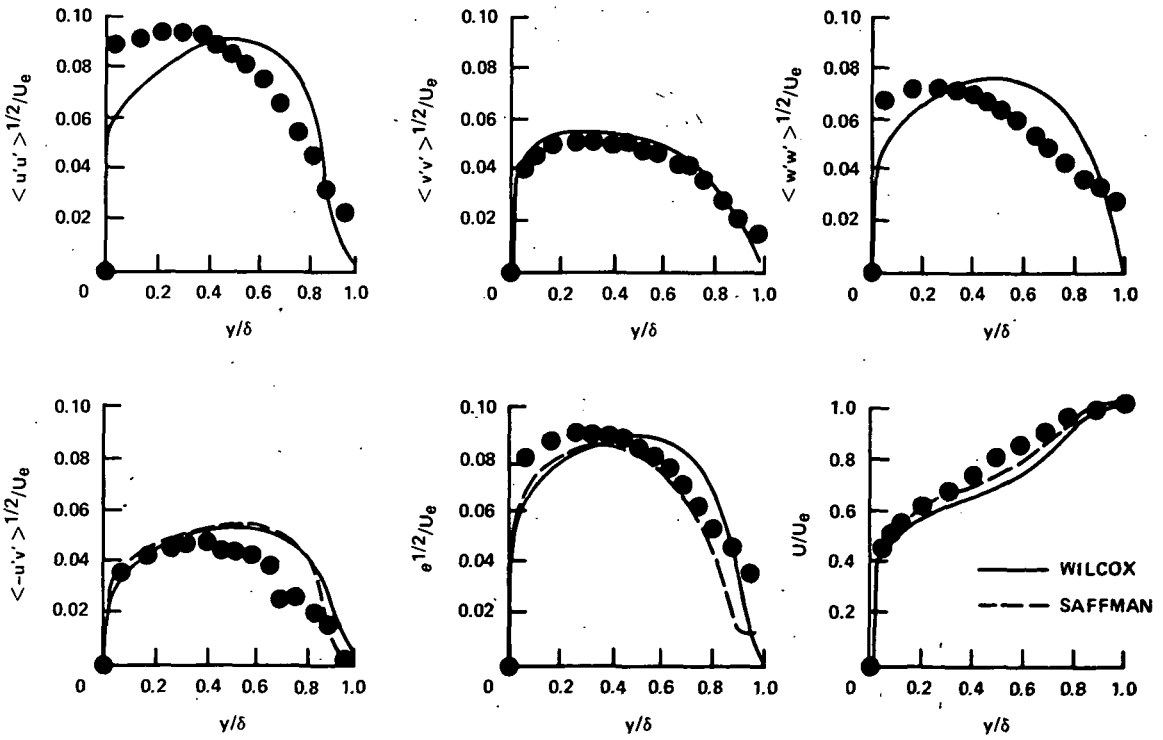

Figure 1. Comparison of Reynolds stress computations with experimental data of Bradshaw (adverse pressure).

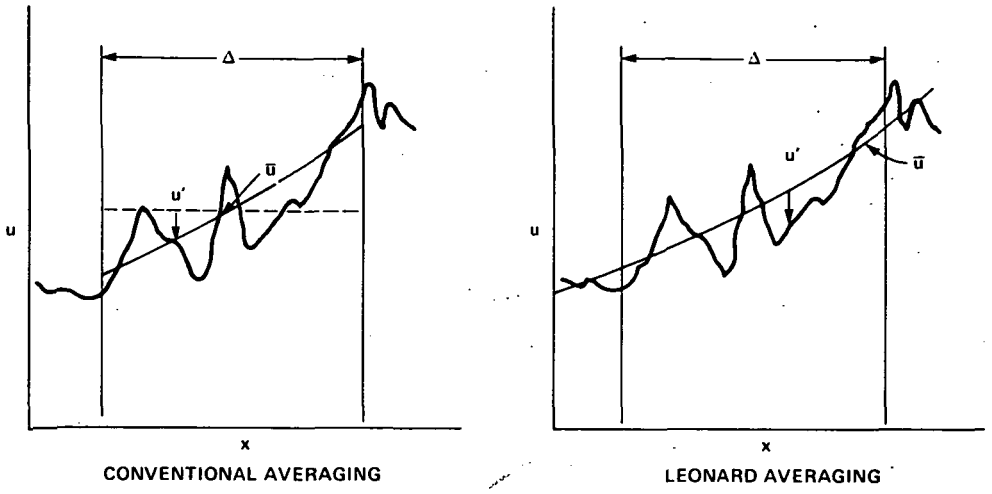

Figure 2. Volume-averaging dependent variables.

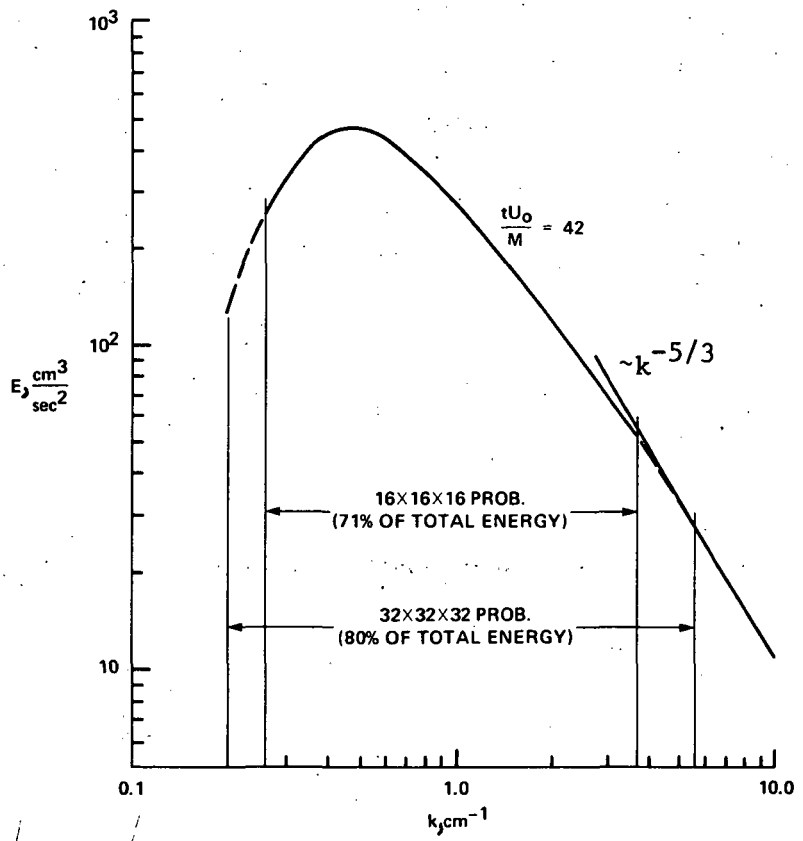

Figure 3. Initial energy spectrum. Data from reference 16.

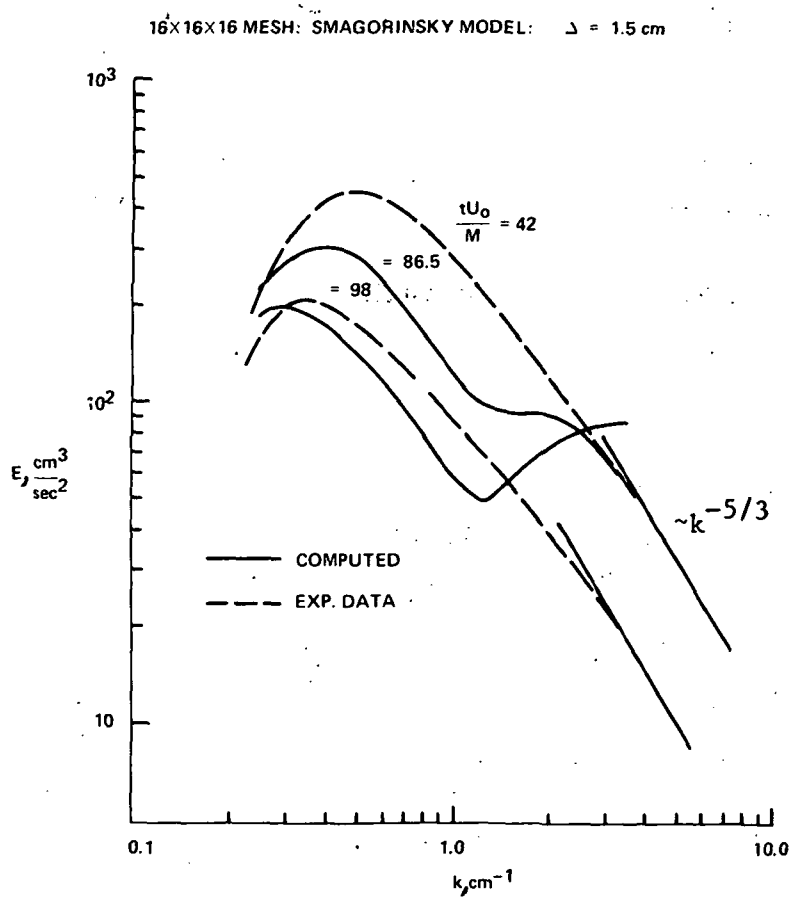

Figure 4. Evolution of energy spectra, $\Delta_{avg} = 0$.

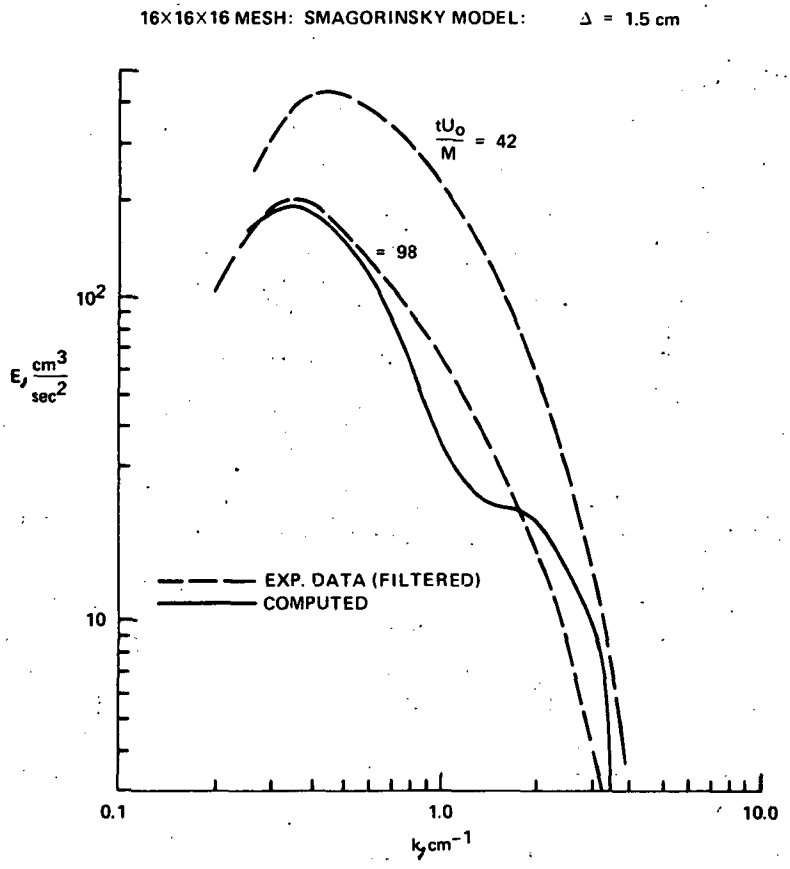

Figure 5. Evolution of energy spectra, $\Delta_{avg} = \Delta$.

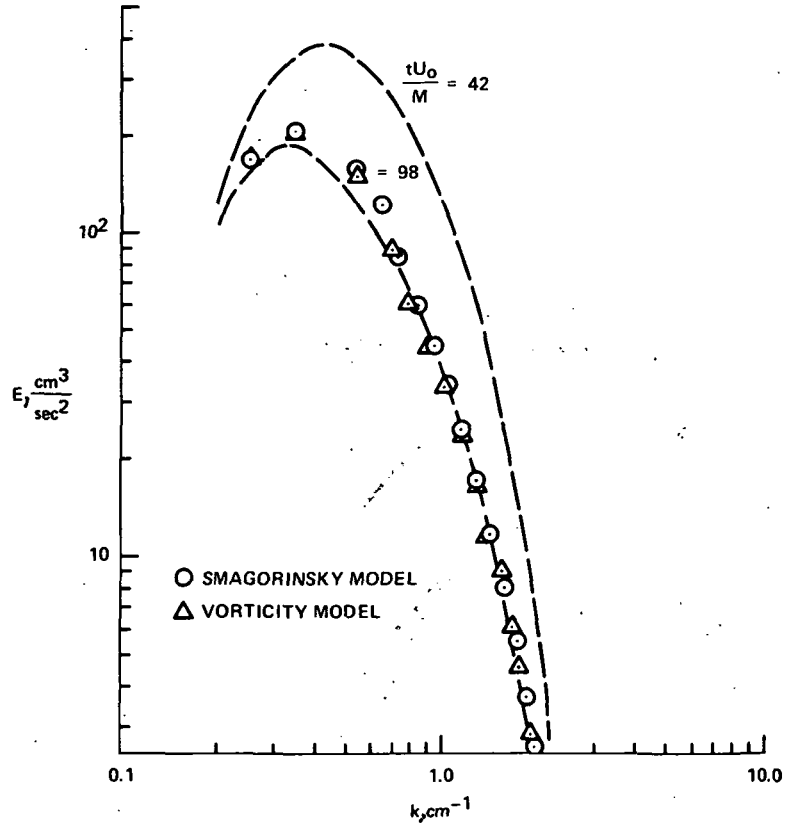

Figure 6. Evolution of energy spectra, $\Delta_{avg} = 2\Delta$.

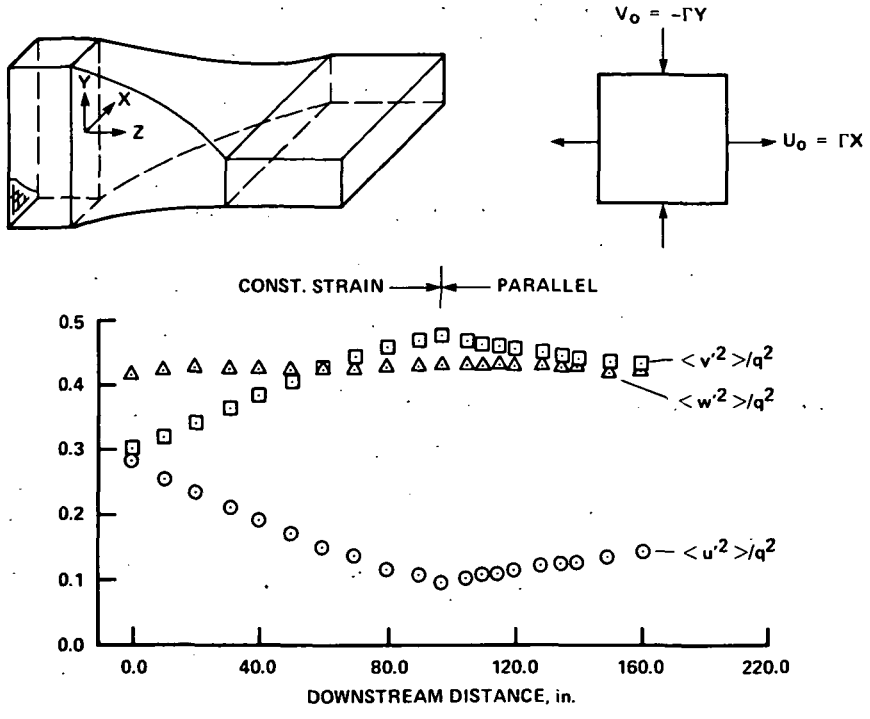

Figure 7. Distortion of homogeneous turbulence by irrotational plane strain.